

Multiplicity and pseudorapidity distribution of photons in S+Au reaction at 200A GeV

M. M. Aggarwal,¹ A. L. S. Angelis,² V. Antonenko,³ T. C. Awes,⁴ S. K. Badyal,⁵ C. Barlag,⁶ K. B. Bhalla,⁷ V. S. Bhatia,¹ C. Blume,⁶ D. Bock,⁶ E.-M. Bohne,⁶ D. Bucher,⁶ A. Buijs,⁸ S. Chattopadhyay,⁹ A. Clausen,⁶ G. Clewing,⁶ A. C. Das,⁹ P. Devanand,⁵ P. Dönni,² E. Durieux,² M. R. Dutta Majumdar,⁹ S. Fokin,³ M. S. Ganti,⁹ S. Garpman,¹⁰ F. Geurts,⁸ T. K. Ghosh,⁹ R. Glasow,⁶ S. K. Gupta,⁷ H.-Å. Gustafsson,¹⁰ H. H. Gutbrod,^{11,*} M. Hartig,⁶ Xiaochun He,¹² G. Hölker,⁶ M. Ippolitov,³ M. Izycki,² S. Kachroo,⁵ R. Kamermans,⁸ K.-H. Kampert,^{6,†} K. Karadjev,³ B. W. Kolb,¹¹ V. Kumar,⁷ I. Langbein,¹¹ J. Langheinrich,⁶ A. Lebedev,³ H. Löhner,¹³ V. Manko,³ M. Martin,² I. S. Mittra,¹ H. Naef,² S. K. Nayak,⁹ T. K. Nayak,¹¹ S. Nikolaev,³ J. Nystrand,¹⁰ F. E. Obenshain,⁴ A. Oskarsson,¹⁰ I. Otterlund,¹⁰ T. Peitzmann,⁶ F. Plasil,⁴ M. Purschke,¹¹ S. Raniwala,⁷ N. K. Rao,⁵ L. Rosselet,² B. Roters,¹¹ J. M. Rubio,² S. Saini,⁴ S. Sambyal,⁵ R. Santo,⁶ H. R. Schmidt,¹¹ T. Siemiarczuk,¹⁴ R. Siemssen,¹³ B. C. Sinha,⁹ S. Slegt,¹³ K. Söderström,¹⁰ N. Solomey,² S. P. Sorensen,¹² G. Stefanek,¹⁴ P. Steinhäuser,¹¹ E. Stenlund,¹⁰ A. Ster,² D. Stüken,⁶ M. D. Trivedi,⁹ C. Tvenhoefel,⁸ N. Van Eijndhoven,⁸ W. H. Van Heeringen,⁸ A. Vinogradov,³ Y. P. Viyogi,⁹ S. Weber,^{6,‡} and G. R. Young⁴

(WA93 Collaboration)

¹Panjab University, Chandigarh 160014, UT, India

²University of Geneva, CH-1211 Geneva 4, Switzerland

³Kurchatov Institute, RU-123182 Moscow, Russia

⁴Oak Ridge National Laboratory, Oak Ridge, Tennessee 37831-6372

⁵University of Jammu, Jammu 180001, India

⁶University of Münster, D-48149 Münster, Germany

⁷University of Rajasthan, Jaipur 302004, Rajasthan, India

⁸Universiteit Utrecht/NIKHEF, NL-3508 TA Utrecht, The Netherlands

⁹Variable Energy Cyclotron Centre, Calcutta 700 064, India

¹⁰University of Lund, S-223 62, Sweden

¹¹Gesellschaft für Schwerionenforschung (GSI), D-64220 Darmstadt, Germany

¹²University of Tennessee, Knoxville, Tennessee 37996

¹³KVI, University of Groningen, NL-9747 AA Groningen, The Netherlands

¹⁴Institute for Nuclear Studies, PL-00681 Warsaw, Poland

(Received 8 May 1997)

The photon multiplicity has been measured for the first time in S+Au collisions at 200A GeV over a wide pseudorapidity range ($2.8 \leq \eta \leq 5.2$) employing a fine granularity preshower detector. The pseudorapidity density of photons increases with centrality, reaching ~ 200 at the highest centrality studied. The results are compared with measurements of the charged particle multiplicity and with predictions of the VENUS event generator. [S0556-2813(98)03407-4]

PACS number(s): 25.75.-q, 24.85.+p

I. INTRODUCTION

The rapid growth of interest in the study of ultrarelativistic nuclear collisions has resulted from the motivation that hadronic matter may undergo a phase transition to quark-gluon plasma if the energy density attained in the collision zone is sufficiently high [1,2]. The energy density can be estimated from the measurement of the transverse energy produced in the reaction or equivalently from the multiplicities of produced particles [3]. Multiplicity and pseudorapidity¹ (η) distributions of particles produced in ultrarelativistic heavy ion collisions also provide valuable informa-

tion on the geometry and the dynamics of the collision [1,2]. Understanding the effects of geometry in terms of the basic nucleon-nucleon and nucleon-nucleus processes is crucial to the isolation of collective effects which might be responsible for the phase transition. Detailed measurements of pseudorapidity distributions are necessary to study fluctuations or intermittency effects and other special event characteristics supposedly accompanying the phase transition [4,5].

The multiplicity and the pseudorapidity distributions of charged particles have been extensively studied at AGS and SPS energies in nucleon-nucleon, nucleon-nucleus, and nucleus-nucleus collisions [1]. In the case of nucleus-nucleus collisions, most of the results can be explained by Monte Carlo models based on string fragmentation [2]. Inclusion of the effects of rescattering has been found to be necessary to describe some features of the data obtained in counter experiments.

In the case of measurements of charged particles in counter experiments, one common complication for interpretation is the simultaneous detection of spectator protons. This problem is usually avoided by measuring the negatively charged particles. An alternative solution is to measure pho-

*Current address: SUBATECH, Ecole des Mines, Nantes, France.

†Current address: University of Karlsruhe, D-76131 Karlsruhe, Germany.

‡Current address: Forschungszentrum Jülich, Germany.

¹Pseudorapidity η ($= -\ln|\tan \theta/2|$) is equal to the rapidity y ($= -0.5 \ln[(E-p_L)/(E+p_L)]$) for massless particles. Since our sample includes some contamination with nonphoton showers, we shall use η throughout this paper.

tons which arise mainly as decay products of the produced particles. Unlike the charged particle multiplicity, however, the photon multiplicity has not been extensively studied in heavy ion reactions.

Photon production in ultrarelativistic heavy ion collisions has traditionally been studied using electromagnetic calorimeters [6], measuring total energy and angle of the particles. In regions of low particle density ($\eta < 2$) it has also been measured using the conversion method [7]. However, in the forward rapidity region, where the particle density is very high, it becomes difficult to use calorimeters because of the large overlap of showers or due to the increase in cost. Thus there has been no published data on the multiplicity and pseudorapidity distribution of photons over a sizable fraction of phase space.

One can study photon production in the forward hemisphere in a restricted way by utilizing a preshower detector of high granularity, and measuring the multiplicity and the pseudorapidity distribution of photons. In the case of ultrarelativistic heavy ion collisions, the photon multiplicity can also be used for global event characterization, e.g., for impact parameter selection and for the study of event shapes and the dynamics of particle production.

The comparison of photon multiplicity and charged particle multiplicity measured in a common part of the phase space on an event-by-event basis promises to explore exciting areas in the mechanism of particle production in nuclear collisions. Several theoretical predictions have been made for the occurrence of large isospin fluctuations arising due to the formation of disoriented chiral condensates [8] and other phenomena [9] accompanying the phase transition. Certain cosmic-ray observations already suggest the occurrence of such isospin fluctuations [10].

In a normal nuclear collision governed by the superposition of independent nucleon-nucleon collisions, it is expected that $N_{\pi^+} \sim N_{\pi^-} \sim N_{\pi^0}$. Assuming $N_{\text{ch}} \sim N_{\pi^+} + N_{\pi^-}$ and $N_{\gamma} \sim 2 \times N_{\pi^0}$, the ratio N_{γ}/N_{ch} becomes an important physical observable for the study of isospin fluctuations on an event-by-event basis. In the case of central S+Au collisions at 200A GeV energy, $N_{\text{ch}} \sim 300$ in the forward hemisphere. For such large multiplicities the width of the N_{γ}/N_{ch} distribution will be small, well within 10%. Because of its narrow distribution, one can distinguish processes having significantly different values of N_{γ}/N_{ch} on an event-by-event basis.

In the present article we describe the *first* detailed measurement of the multiplicity and pseudorapidity distribution of photons in $^{32}\text{S}+\text{Au}$ reactions at the SPS in the WA93 experiment [11]. The data were taken during the sulphur beam runs in 1991 and 1992. Preliminary results have been presented earlier [12]. Section II describes briefly the WA93 experimental setup and the preshower photon multiplicity detector (PMD). Procedures for data analysis along with the estimation of photon counting efficiencies, associated background, and the related errors are described in Sec. III. Results on multiplicity and pseudorapidity distributions of photons are presented in Sec. IV. Discussion of the results in light of charged particle measurements and a summary are presented in the last section.

II. WA93 EXPERIMENT

The detector subsystems employed in the WA93 experiment have been described in detail elsewhere [13–17]. A

250 mg/cm² thick Au target was used in the experiment. In the following we briefly describe the WA93 experimental setup and the detectors relevant to the data analysis and the results presented in this article.

A. General layout

The major goal of the WA93 experiment at the CERN SPS has been to observe and correlate different signatures of the formation of quark-gluon plasma in several classes of events which are based on both hadron and photon measurements [11]. Figure 1(a) shows the layout of the WA93 experiment at the H3 beam line of the CERN SPS. The experiment consisted of three main subsystems: (i) the charged particle tracking and momentum measurement devices using a combination of multiple step avalanche chambers [16] and the Goliath magnet, and the silicon drift detector (SDD) for the charged particle multiplicity measurement, (ii) the photon measurement subsystem employing three arrays of lead glass calorimeter [15] and a PMD [17] sandwiched between the calorimeters in the forward hemisphere as shown in Fig. 1(b), and (iii) the trigger subsystem consisting of a set of beam defining counters, the midrapidity calorimeter (MIRAC) [13] measuring the transverse energy E_T , and the zero-degree calorimeter (ZDC) [14] measuring the forward energy E_{ZDC} of the beam spectators. On-line selection of centrality of the collision was provided by the transverse energy E_T measured in the MIRAC. The trigger subsystem and the lead glass calorimeter were the same as used in the WA80 experiment.

B. Photon multiplicity detector

The preshower PMD is based on the principle that in converters of moderately small thickness (a few radiation lengths) the hadrons mostly behave as minimum ionizing particles (MIP's) whereas photons are much more likely to initiate a shower and produce larger signals in the sensitive medium. In addition the preshower should have appreciable transverse size in comparison to minimum ionizing hadrons. Thus photon preshowers can be distinguished from those of hadrons if the detector possesses adequate granularity and can record information on both the magnitude and the spatial distribution of energy deposition.

1. Hardware

The PMD consisted of a rectangular matrix of 7500 plastic scintillator pads of size $20 \times 20 \times 3$ mm³ placed behind a $3X_0$ thick lead converter plate and divided into four quadrants surrounding the beam pipe. The light from the pads was transported via 1 mm diameter wavelength shifting plastic fibers to the image intensifier-charge coupled device (CCD) camera readout devices [18]. Four CCD cameras, obtained from the UA2 experiment, were used for the four quadrants. The lead plates and the cameras were supported on a 6 mm thick steel plate forming part of a light-tight box in which the entire assembly was enclosed.

The scintillator pads in each quadrant were arranged in the form of a rectangular matrix having 38 rows and 50 columns. Room for the beam pipe was made by removing 5×5 pads from each quadrant. The output ends of the wavelength shifting fibers were arranged in exactly the same ma-

WA93

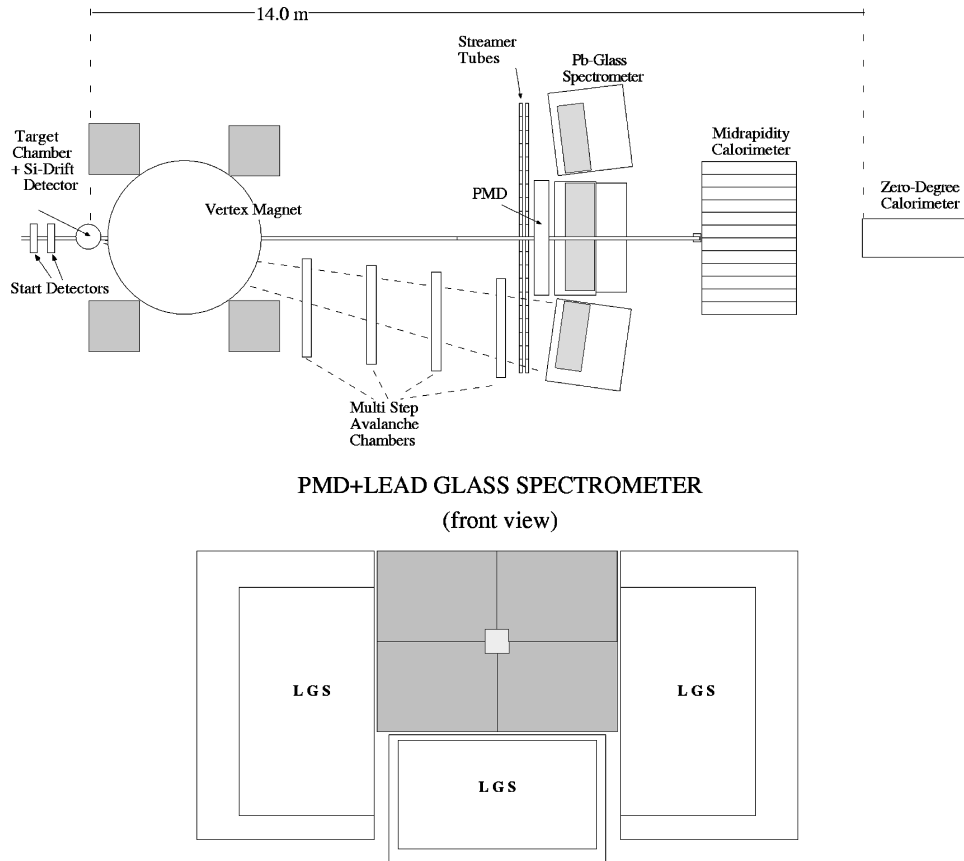


FIG. 1. Layout of the WA93 experiment: (top) lateral view of all the subsystems, (bottom) front view of the photon subsystem showing the PMD (shaded region) in the forward hemisphere surrounded by the lead glass spectrometers.

trix and were coupled to one readout device. The three-stage image intensifier chain provided light amplification of $\sim 40\,000\times$. The correspondence between the pad coordinates in the detector and the pixel coordinates of the CCD camera was established by using a set of fiducial pads in each quadrant. These fiducial pads had one extra clear fiber inserted in addition to the wavelength shifting fiber to selectively launch light into the pads using an externally triggered light source. A map assigning each pixel to a fiber (called a pixel-to-fiber map) was generated using data on fiducial fibers to transform the CCD pixel coordinates to a suitable fiber coordinate system. The CCD pixel charge was digitized using an 8-bit custom-built fastbus digitizer. A hardware threshold of two analog-to-digital converter (ADC) channels at the pixel level was set to remove the electronic noise. The digitized signals of those pixels, which were above the hardware threshold after pedestal subtraction and belonged to a particular fiber, were summed and these compressed data were recorded for off-line analysis.

The details of the PMD, its readout devices, and the data taking modes can be found in [17].

2. Acceptance

The PMD was placed at a distance of 10.09 m from the target and covered the pseudorapidity region $2.8 \leq \eta \leq 5.2$. The variation of the azimuthal coverage as a function of

pseudorapidity is shown in Fig. 2(a). The region $3.3 \leq \eta \leq 4.9$ had full azimuthal acceptance. The efficiency of the PMD for the lower range of p_T values of the detected photons, as deduced from simulation, is shown in Fig. 2(b). It is seen that the p_T acceptance of photons in the PMD extends to quite low (~ 20 MeV) values. The two-track resolution, corresponding to a 3 cm distance on the PMD plane, varied from 0.03 units of pseudorapidity in the outer regions of the detector to 0.25 units in the innermost region near the beam.

III. DATA REDUCTION AND ANALYSIS

A. Data reduction

The following procedure was adopted to reduce the data to obtain particle hit positions and the energy deposition signal for subsequent physics analysis.

The data comprising the pad signals of the four quadrants were combined and transformed to a 76×100 pad matrix. To take care of the variation in the response of individual pads, the raw digitized signals from the pads were multiplied by the pad-to-pad normalization factors determined earlier [17]. The matrix of signal values for each event was then passed through a clustering routine which unfolded the overlapping hits, calculated the centroid of the clusters, and assigned a total signal strength to the clusters. Those clusters having signals below a predetermined threshold were rejected as

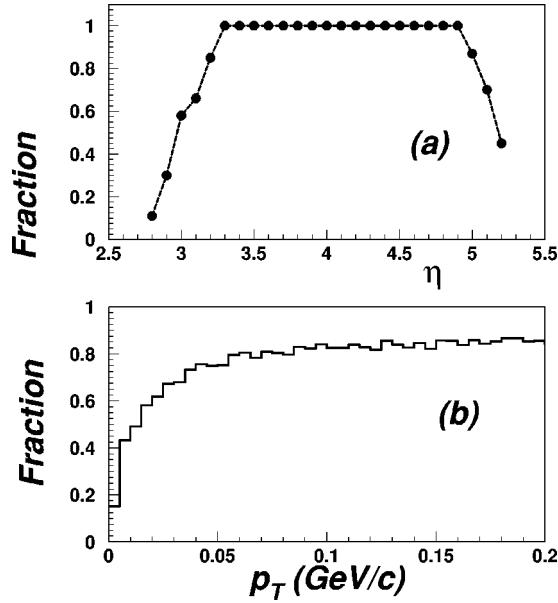


FIG. 2. (a) Fractional acceptance in azimuth as a function of pseudorapidity and (b) photon detection efficiency of the PMD for the lower range of p_T values.

originating mainly from hadrons behaving like minimum ionizing particles, and those above the threshold were labeled as “ γ -like clusters,” originating predominantly from photons [17]. A fraction of the clusters originating from hadronic interactions in the converter material, photon conversions in upstream materials, and scattering of particles from outside the region of acceptance of the PMD constituted the background.

The photon multiplicity (N_γ) is obtained from the multiplicity of γ -like clusters (N'_γ) using the relation

$$N_\gamma = \frac{N'_\gamma - N_b}{\epsilon_\gamma},$$

where ϵ_γ represents the photon counting efficiency and N_b is the number of background clusters in the event.

Using the VENUS event generator [19] and the GEANT simulation package [20] used to describe the complete WA93 experimental setup, the various steps in the data reduction, e.g., clustering, efficiency, and background, have been studied in detail as a function of centrality and pseudorapidity. VENUS particles in the full angular range of WA93 acceptance were used for this study. The GEANT results on energy deposition in pads were converted to the digitized signals by adjusting parameters to reproduce the test beam data as described in Ref. [17]. Assuming that the hadron production in S + Au reactions at SPS energy is described by VENUS, the average number of background clusters was obtained from simulation and used for subtraction in the above relation. This assumption is well justified in view of the agreement of the experimental multiplicity and pseudorapidity distributions of charged particles in S + Au collisions at the SPS [24] with the VENUS results.

B. Event selection

For the presentation of the results as a function of centrality, the selection was based on the total transverse energy E_T

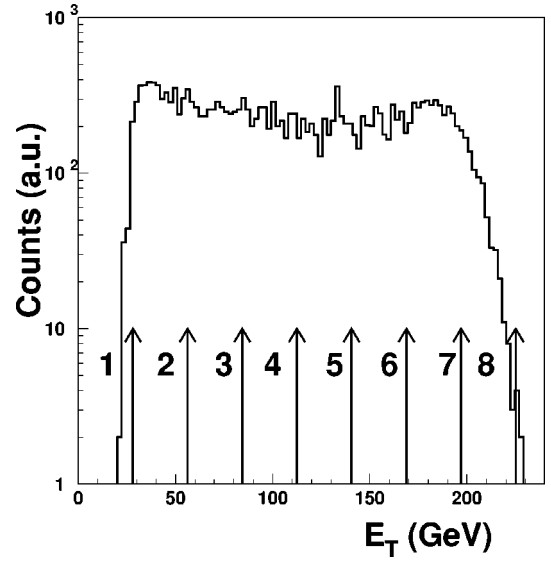


FIG. 3. Histogram of transverse energy E_T measured by the MIRAC showing the eight different centrality bin selections. (Bins 2, 3, 4, 5, 6, 7, and 8 represent 20%, 15%, 13%, 13.2%, 13.6%, 15.5%, and 7% of minimum bias cross sections, respectively.)

measured by the MIRAC as shown in Fig. 3. The minimum bias trigger corresponds to $E_T > 20$ GeV. The entire E_T range has been divided into eight equal bins, as shown in the figure, for the study of the centrality dependence of the measured photon multiplicity and pseudorapidity distributions. The extreme peripheral data (bin 1) have not been analyzed. For the discussions in subsequent sections the “peripheral” sample corresponds to bin 2 and the “central” sample corresponds to bin 8.

C. Study of pseudorapidity and centrality dependence of efficiency and background

1. Photon counting efficiency

The total photon counting efficiency ϵ_γ depends on several factors, e.g., the energy spectrum of photons, the conversion probability, the hadron rejection threshold applied, the granularity, and the associated clustering efficiency. This can be described as a convolution of two components: (a) the conversion probability (ϵ_{conv}) and (b) the clustering efficiency (ϵ_{cls}). It is instructive to study the dependence of these components on the centrality and the pseudorapidity to gain insight into the capability of the PMD for measuring the multiplicity and pseudorapidity distributions of photons in the high particle density environment of heavy ion experiments.

a. Conversion probability ϵ_{conv} . Photons initiating a pre-shower are said to be converted if the signal in the detector due to the shower particles is above the noise level in all the affected pads. For very low energy photons the shower particles are either absorbed in the thick converter or produce a small signal below the noise threshold in each pad. In the present discussion the conversion probability is defined as the fraction of the number of photons producing signals above the hadron rejection threshold.

The conversion probability (ϵ_{conv}) as a function of η was obtained by the ratio of the number of photons tracked with

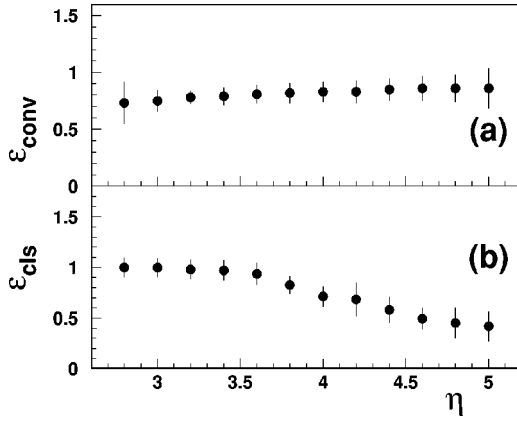


FIG. 4. Pseudorapidity dependence of (a) conversion probability and (b) clustering efficiency for central events. Vertical bars represent the rms spread in the mean values.

GEANT above threshold to the number of incident photons on the detector. Figure 4(a) shows the variation of ϵ_{conv} with η for the central event class. The vertical bars represent the rms spread in the ratio in the various η bins. The conversion probability increases slightly with higher η because of the rapidity boost of the photons.

b. The clustering efficiency (ϵ_{cls}). Because of the high particle multiplicity, there is some overlap of clusters even in a preshower detector. The clustering algorithm in general cannot resolve all overlapping clusters. In addition there is a possibility that a large single cluster may be split into two or more clusters due to shower fluctuations or imperfections in the clustering algorithm. It is therefore necessary to study the clustering efficiency, which is defined as the ratio of the number of clusters found at the output stage of the algorithm to the input number of photons.

The clustering efficiency has been studied by two different methods: (a) by simulation, where the number of particles (the GEANT tracks) producing signals above the hadron rejection threshold was taken as the input number of clusters, and (b) by a mixed event method, where peripheral trigger events of low multiplicity (<30) taken from the experimental data were overlaid to generate synthetic events resembling high multiplicity central events [21]. In the case of simulation the input number of clusters is known exactly while in the case of synthetic events there may be a small uncertainty if the clustering algorithm had less than perfect efficiency for the peripheral events. On the other hand, the synthetic events, having been derived from experimental data, represent the effects of readout more realistically than the simulated events even though a detailed procedure was adopted to tune the simulation to the experimental data. Thus the two methods should complement each other.

While generating synthetic events, care was taken to match the mean total number of γ -like clusters and the total signal sum of such clusters in the synthetic events to those of the experimental data for any given centrality. This allows us to estimate the efficiency for the highest observed particle density. To take care of possible differences in the pseudorapidity distribution of peripheral and central events, an analysis with synthetic events was performed for $\delta\eta=0.2$ units of pseudorapidity over the entire range. The total signal sum and the number of clusters in the synthetic events were

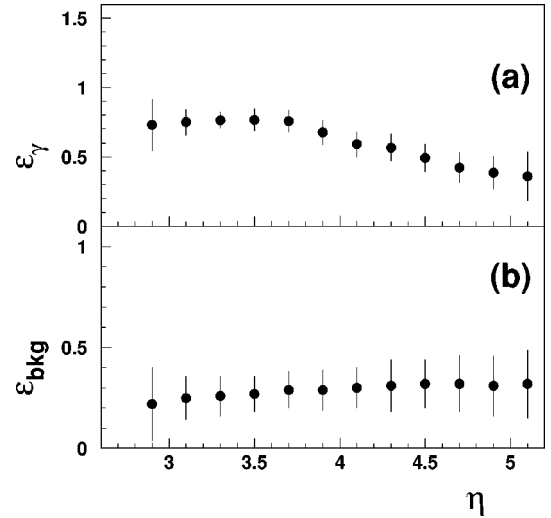


FIG. 5. Pseudorapidity dependence of (a) photon counting efficiency ϵ_{γ} and (b) background fraction ϵ_{bkg} for central events. Vertical bars represent rms spread in the mean values.

matched for every bin with those in the experimental data.

The dependence of the clustering efficiency on pseudorapidity is shown in Fig. 4(b) for the case of central events. The results of the two methods compare well, the values used in the analysis being those obtained from simulation studies and the difference being assigned to systematic error as described later. The clustering efficiency reduces as one moves to higher η regions. This is due to the increased particle density and the resulting increase in the overlap of clusters.

c. Pseudorapidity and centrality dependence of ϵ_{γ} . Having determined the variation of ϵ_{conv} and ϵ_{cls} with η as described above, one can easily deduce the η dependence of ϵ_{γ} . This is shown in Fig. 5(a) for the case of central events. The bars shown represent the rms spread in the average value. The photon counting efficiency in central events is found to be $\sim 75\%$ up to $\eta=3.7$, after which it starts decreasing slowly with increasing η , reaching a value of $\sim 45\%$ at the highest η value covered by the PMD.

By taking weighted average of η -dependent efficiency values, we have calculated ϵ_{γ} for different centralities. The results are presented in Fig. 6(a). The bars shown represent the rms spread in the average value. Here the variation is less rapid with centrality, falling from $\sim 80\%$ for the peripheral sample studied to about $\sim 67\%$ for extreme central events.

2. Background fraction ϵ_{bkg}

A major source of background to the identified photons comes from incident hadrons which either interact in the converter and produce large signals or have signals in the long Landau tail which get included in the γ -like clusters even after applying the threshold for hadron rejection. A minor contribution to the background also arises from scattering of particles from outside the cone of acceptance of the PMD, upstream conversion of photons in air and other materials, and because of the splitting of clusters.

The background fraction $\epsilon_{\text{bkg}}=N_b/N'_{\gamma}$ has been estimated using simulation as described in [17]. Figure 5(b) shows the variation of ϵ_{bkg} as a function of η for central S+Au events.

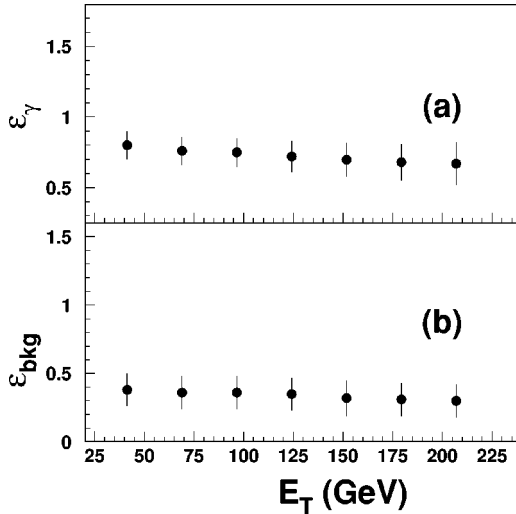


FIG. 6. Centrality dependence of (a) photon counting efficiency ϵ_γ and (b) background fraction ϵ_{bkg} . The horizontal axis shows the transverse energy E_T . Vertical bars represent rms spread in the mean values.

The bars correspond to the rms spread in the value. The dependence of ϵ_{bkg} on centrality is shown in Fig. 6(b). In both cases, the values lie within a band of 30%–40%. It is found that the fractional contribution of background increases only slightly as one moves from central to peripheral collisions and when one goes to forward pseudorapidity regions.

D. Errors

The statistical error on the photon multiplicity is small compared to the systematic error. The possible sources of systematic errors and their contributions to the photon counting efficiency and the background fraction are discussed here.

The largest contribution to the systematic error in the photon counting efficiency arises from the uncertainty in the estimation of the clustering efficiency. While generating synthetic events from peripheral data, it is difficult to judge the clustering inefficiency for the peripheral data itself. To reduce the effect we choose peripheral events of the lowest multiplicity to generate synthetic events. While superposing the events, the incidence of more than one track on the same pad will result in an overlap and loss of clusters. There is a possibility of more than one subthreshold cluster forming the “ γ -like cluster” due to overlap. A large cluster can also be split into more than one cluster. For central S+Au events in the outer regions of the PMD, i.e., at lower η , the estimated error due to this effect on the photon counting efficiency is less than 5%, while for the highest η region the error goes up to 9%. For peripheral events the systematic error on the photon counting efficiency is less than 5%.

The photon counting efficiency is calculated using the VENUS event generator. If the experimental energy and p_T distributions are not described well by VENUS, there may be some uncertainty in the extracted values of ϵ_γ . There are indications of an enhancement of the photon spectrum at low p_T [23]. Although the p_T acceptance of the PMD extends to quite low values, as shown in Fig. 2(b), the integrated photon

counting efficiency may change slightly if the p_T spectrum changes. Using the photon p_T spectrum of [23] the photon counting efficiency decreases by about 4% as compared to that obtained from VENUS simulations.

The following sources contribute to uncertainties in the estimation of the background fraction.

(i) Particles outside the cone of the PMD can get scattered in the upstream materials (air, beampipe, and other structural materials) and produce hits on the PMD. This is estimated by the number of additional tracks outside the PMD geometry producing γ -like clusters. For most central collisions at the most 5% of γ -like clusters come from this source.

(ii) Upstream conversion of photons and splitting of clusters amount to less than 2% of the total γ -like clusters.

(iii) The estimation of the systematic error on the background fraction due to the possible variation in the hadronic fraction in the event has been obtained using two different event generators (VENUS and FRITIOF [22]). The ϵ_{bkg} values obtained differ by less than 5%, which corresponds to an uncertainty of less than 2% in N_γ .

The overall correction factors applied to the multiplicity of “ γ -like clusters” obtained from the simulation and the synthetic event methods discussed earlier differ at the most by about 6%. The results discussed here are the values obtained by using the synthetic event generation method to obtain the clustering efficiencies at various η bins. The difference from the averages is included in the overall systematic error, which increases somewhat for the larger η regions.

The combined systematic error on the photon multiplicity is 10% for peripheral events and is almost independent of the pseudorapidity range considered. For central events the upper limit on the systematic error is 12.5%, being slightly less for the smaller pseudorapidity region.

IV. MULTIPLICITY AND PSEUDORAPIDITY DISTRIBUTIONS OF PHOTONS

A. Multiplicity distribution of photons

The minimum bias distribution of the photon multiplicity N_γ for the pseudorapidity region $3.3 \leq \eta \leq 4.8$ is shown in Fig 7. This region has been selected because of full azimuthal coverage. The data have been corrected for interactions of the beam with material other than the target by subtracting suitably normalized results from runs taken with an empty target. The correction was $\sim 10\%$ in the peripheral region and negligible for central events. The horizontal bars represent the systematic error in the determination of N_γ . The extreme peripheral portion of the spectrum corresponding to $N_\gamma < 20$ has not been plotted because of the trigger cut applied to the peripheral data. The shape of the distribution is essentially determined by the collision geometry. The plateau stems from collisions with intermediate impact parameters while the knee at high multiplicity corresponds to the range of impact parameters where all of the projectile overlaps with the target, a well-known characteristic of asymmetric collisions [24]. The tail region has a Gaussian shape, as shown by the dashed line fit, resulting from fluctuations in the number of participants when the overlap of nuclei is complete.

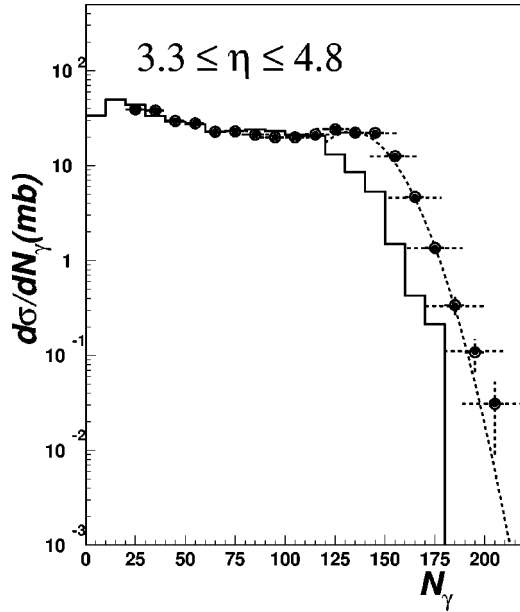


FIG. 7. Minimum bias distribution of photon multiplicity N_γ . The horizontal bars indicate the extent of the systematic errors on N_γ . The solid line represent the VENUS results for comparison. The dashed line shows a Gaussian fit to the tail region.

Predictions of the VENUS event generator, version 3.11 [19], with rescattering is superimposed on Fig. 7 for comparison. No attempt has been made to tune the parameters of VENUS to reproduce the data. It is seen that there is a general agreement in the shape of the minimum bias distributions from the experiment and from VENUS. However, the event generator with default parameters underpredicts the photon multiplicity as also seen in the case of charged particle multiplicity [24].

B. Correlation between E_T , E_{ZDC} , and N_γ

The multiplicity of produced particles in heavy ion collisions directly depends on the impact parameter, or centrality, of the collision. Hence it is instructive to study the correlation of N_γ with the centrality information obtained from the trigger detectors, e.g, the total transverse energy (E_T) from the MIRAC and the energy deposited in the ZDC (E_{ZDC}). Figure 8 shows such a correlation. As expected, the photon multiplicity is seen to increase with the increase in centrality, which is represented by the increase in the transverse energy or the decrease in the ZDC energy. This clearly demonstrates that N_γ is a useful global observable which can be used for event selection. A tiny fraction (0.2%) of events attributed to background are found to deviate from the linear behavior. They do not affect the inclusive results discussed in this article.

C. Pseudorapidity distribution of photons

The pseudorapidity distribution of photons for S+Au collisions is shown in Fig. 9 for three centrality ranges, central (highest E_T bin), peripheral (second lowest E_T bin), and intermediate (fifth E_T bin). The data have been corrected for geometry, photon counting efficiency, and background. The pseudorapidity bin width of $\Delta\eta = 0.2$ units is selected such that it is large compared to the two-track resolution in most

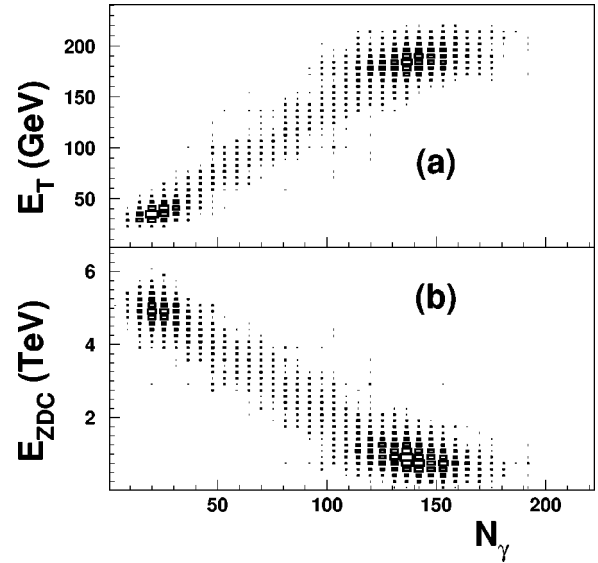


FIG. 8. Correlation of the photon multiplicity N_γ with (a) the transverse energy E_T and (b) the forward energy E_{ZDC} in the event.

parts of the detector. The horizontal error bars display the uncertainty in the η assignment due to a worsening two-track resolution at larger η values. The vertical error bars include systematic and statistical errors, the latter being usually much smaller compared to the former.

The predictions of the VENUS (version 3.11) event generator are superposed on Fig. 9 for comparison. To obtain impact parameter selection comparable to the experimental data, the total transverse energy spectrum of the VENUS particles falling within the MIRAC geometry has also been divided into eight equal bins like that for the experimental data. The shape of the pseudorapidity distribution obtained from VENUS matches the data reasonably well. However, the event generator underestimates the multiplicity.

A Gaussian fit to the pseudorapidity distributions was made to extract the maximum value ρ_{\max} , the peak position η_{peak} , and the width σ for different centrality bins. The re-

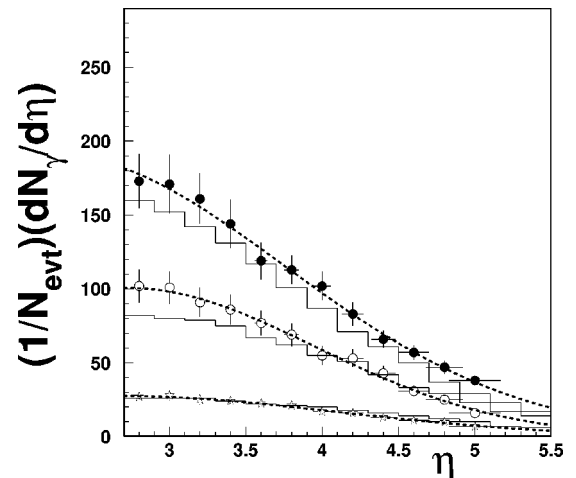


FIG. 9. Pseudorapidity distribution of photons for S+Au collisions at 200A GeV for three different centrality classes (solid circles, open circles, and stars represent E_T bins 8, 5, and 2, respectively). The histograms represent the VENUS results and the dotted line represents the Gaussian fit to the data.

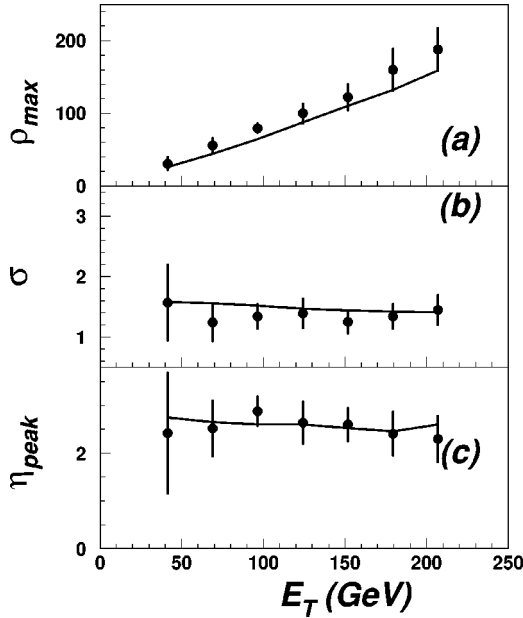


FIG. 10. Variation of the shape parameters describing the pseudorapidity distribution of photons for S+Au collisions for different centralities (defined by E_T). VENUS results for similar centrality classes are superposed for comparison, as shown by the solid lines.

sults are shown in Fig. 10 as a function of E_T . As the coverage of the PMD does not extend up to the peak of the distribution, the uncertainties in the fitted parameters are somewhat large.

It is seen that the pseudorapidity density increases with centrality, going from 30 for peripheral events to 190 for the most central case studied. This is understood to be a consequence of the geometry of the nuclear collision. In the case of the event generator, while the variation is similar, the absolute values are lower than observed in the data. The width of the pseudorapidity distribution of photons varies little with centrality, remaining around 1.4. The overall features of the centrality dependence of σ and η_{peak} are well described by the VENUS event generator.

V. DISCUSSIONS AND SUMMARY

A preshower detector with suitable converter thickness and granularity has been used to measure the multiplicity of photons even in the high particle density environment of heavy ion collisions. The photon multiplicity detector of the WA93 experiment is the first implementation of its kind. The detector has been used to measure both the multiplicity and pseudorapidity distribution of photons in the forward hemisphere in S + Au collisions at 200A GeV.

The present work represents the first large acceptance measurement of the photon multiplicity for this system over a wide range of pseudorapidity and centrality and hence direct comparison with other experiments is not possible. However, it is instructive to compare the present results with those obtained from the measurement of the charged particle multiplicity for the same system in the WA80 experiment [24]. This is useful as the major source of photons is the decay of π^0 's which should be produced in a similar number as charged pions.

The general features of the minimum bias distribution of

photons and the pseudorapidity distributions agree qualitatively well with the results of the charged particle distributions measured by the WA80 Collaboration [24]. The photon pseudorapidity density value of 190 for the highest centrality is seen to be somewhat higher as compared to the value of 175 for charged particles. This can be a consequence of the different centralities in the two works. Whereas WA80 used the zero-degree energy to characterize centrality, the present analysis has used the transverse energy for the same. It has been shown in [24] that such differences in event selection may lead to very different values of ρ_{max} extracted from the data, with the E_T selection always giving higher values than the selection based on a zero-degree trigger. When the centrality selection is tight and corresponds to only a few percent of the total minimum bias cross section, the ρ_{max} values with the E_T selection can be 10% higher than for the zero-degree energy selection. It is also known from pp studies [25] that the pseudorapidity distributions of photons are different from those of charged particles, the photon distributions having higher densities and smaller widths.

The trend of the variation of the width σ and the position of the peak η_{peak} with centrality is not so pronounced as found in large acceptance charged particle measurements [2,24]. The widths in the WA80 work varied from ~ 1.5 to ~ 1.9 for the S+Au case, increasing almost linearly as a function of the zero-degree energy, but the widths of the photon distributions are stable around 1.4. In the HELIOS measurement the width σ was found to vary rather very slowly with E_T [26]. The difference in the behavior of the widths in the emulsion and WA80 studies was explained by possible differences in the sensitivity of the two experiments to charged particles. However, the difference in the variation of the widths with centrality in the case of photon measurements in the present work and charged particle measurements of WA80 mainly arises from the presence of spectator protons in the latter case as also noted in Sec. I. The spectators disappear steadily with increasing centrality, move to smaller absolute rapidities in the c.m., and are overwhelmed by the produced particles for very central events. Thus the increasing width in the WA80 experiment with increasing impact parameter is nicely explained by spectator protons. For photons there is no influence of this spectator matter and hence the rapid change with centrality is almost absent.

The experimental pseudorapidity distribution is found to be somewhat higher than that obtained with the VENUS event generator. A possible explanation for this observation could be the sensitivity of the PMD to low p_T particles, down to ~ 20 MeV/c. The NA44 Collaboration has reported enhancement in the charged particle production at low p_T [27]. In a companion measurement in the WA93 experiment using a BGO calorimeter [23], it is found that a single exponential shape with an inverse slope of 210 MeV is unable to describe the p_T spectrum over the entire range. Inclusion of a second component with an inverse slope of 100 MeV improves the description but even this fails for the lowest p_T values. Because of the exponential shape of the p_T spectra, changes of $\sim 10\%$ in the photon yield can easily result from relatively small changes in the acceptance of the detector in the low p_T region.

In summary the general features of the multiplicity and pseudorapidity distributions of photons measured in S+Au

reactions at the SPS energy compare well with those of charged particles measured in the same system. This lends support to measuring photon multiplicity as a complementary observable to charged particle multiplicity. Measuring the two together on an event-by-event basis in the common part of phase space is useful for the study of isospin fluctuations. This is being attempted in the WA98 experiment [28].

ACKNOWLEDGMENTS

We would like to thank the CERN SPS accelerator crew for providing excellent sulphur beam conditions. This work was supported jointly by the German BMBF and DFG, the

U.S. DOE, the Swedish NFR, the Dutch Stichting FOM, the Humboldt Foundation, the Stiftung für deutsch-polnische Zusammenarbeit, the Department of Atomic Energy, the Department of Science and Technology and the University Grants Commission of the Government of India, the Indo-FRG Exchange Programme, the PPE division of CERN, Swiss National Fund, the International Science Foundation under Contract No. N8Y000, the INTAS under Contract No. INTAS-93-2773, and ORISE. ORNL is managed by Lockheed Martin Energy Research Corporation under Contract No. DE-AC05-96OR22464 with the U.S. Department of Energy.

-
- [1] J. Schukraft and H.R. Schmidt, *J. Phys. G* **19**, 1705 (1993); J. Stachel and G.R. Young, *Annu. Rev. Nucl. Part. Sci.* **44**, 537 (1994); M.J. Tannenbaum, *Int. J. Mod. Phys. A* **4**, 3377 (1989).
 - [2] M.M. Aggarwal and S. I. A. Garpman, *Int. J. Mod. Phys. E* **4**, 477 (1995).
 - [3] J.D. Bjorken, *Phys. Rev. D* **27**, 140 (1983).
 - [4] A. Bialas and R. Peschanski, *Nucl. Phys.* **B273**, 703 (1986).
 - [5] A. C. Das and Y. P. Viyogi, *Phys. Lett. B* **380**, 437 (1996); S.K. Nayak and Y.P. Viyogi, *ibid.* **367**, 386 (1996).
 - [6] R. Albrecht *et al.*, *Phys. Rev. Lett.* **76**, 3506 (1996).
 - [7] HELIOS Collaboration, T. Akesson *et al.*, *Z. Phys. C* **46**, 369 (1990).
 - [8] J. D. Bjorken *et al.*, "Baked Alaska," SLAC Report No. SLAC-PUB-6109, 1993; *Proceedings of Les Rencontres de Physique de la Vallee d'Aoste*, edited by M. Greco (Editions Frontieres, La Thuile, 1993), p. 507; S. Gavin *et al.*, *Phys. Rev. Lett.* **72**, 2143 (1994).
 - [9] S. Pratt, *Phys. Lett. B* **301**, 159 (1993).
 - [10] C.M.G. Lates, Y. Fujimoto, and S. Hasegawa, *Phys. Rep.* **65**, 151 (1980).
 - [11] WA93 Collaboration, Report No. CERN/SPSC/90-14, SPSC/P252, 1990.
 - [12] WA93 Collaboration, Y.P. Viyogi *et al.*, *Nucl. Phys.* **A556**, 623c (1994).
 - [13] T.C. Awes *et al.*, *Nucl. Instrum. Methods Phys. Res. A* **279**, 479 (1989).
 - [14] G.R. Young *et al.*, *Nucl. Instrum. Methods Phys. Res. A* **279**, 503 (1989).
 - [15] H. Baumeister *et al.*, *Nucl. Instrum. Methods Phys. Res. A* **292**, 81 (1990).
 - [16] I. Izycki *et al.*, *Nucl. Instrum. Methods Phys. Res. A* **310**, 98 (1991).
 - [17] M.M. Aggarwal *et al.*, *Nucl. Instrum. Methods Phys. Res. A* **372**, 143 (1996).
 - [18] R.E. Ansorge *et al.*, *Nucl. Instrum. Methods Phys. Res. A* **265**, 33 (1988); J. Aliti *et al.*, *ibid.* **279**, 364 (1989).
 - [19] K. Werner, *Phys. Rev. Lett.* **62**, 2460 (1989).
 - [20] R. Brun *et al.*, "GEANT3 user's guide," Report No. CERN/DD/EE/84-1, 1984.
 - [21] S. Chattopadhyay, Ph.D. thesis, Calcutta University, 1996.
 - [22] B. Nilsson-Almqvist and E. Stenlund, *Comput. Phys. Commun.* **43**, 387 (1987).
 - [23] WA93 Collaboration, M.M. Aggarwal *et al.*, *Phys. Rev. C* **56**, 1160 (1997).
 - [24] R. Albrecht *et al.*, *Z. Phys. C* **55**, 539 (1992).
 - [25] UA5 Collaboration, R.E. Ansorge *et al.*, *Z. Phys. C* **43**, 75 (1989).
 - [26] HELIOS Collaboration, T. Akesson *et al.*, *Nucl. Phys.* **B342**, 279 (1990).
 - [27] NA44 Collaboration, H. Boggild *et al.*, *Z. Phys. C* **69**, 621 (1996).
 - [28] WA98 Collaboration, T.K. Nayak *et al.*, in *Proceedings of the International Conference on Physics and Astrophysics of Quark-Gluon Plasma (ICPA-QGP'97)*, edited by B.C. Sinha, D.K. Srivastava, and Y.P. Viyogi (Narosa Publishing House, New Delhi, in press).